FROM MAGNONS TO THE RESONANCE PEAK: SPIN DYNAMICS IN HIGH-T_C SUPERCONDUCTING CUPRATES BY INELASTIC NEUTRON SCATTERING

Philippe Bourges

Laboratoire Léon Brillouin,
CEA-CNRS, CE Saclay,
91191 Gif sur Yvette, France

1. INTRODUCTION

Over the last decade, inelastic neutron scattering (INS) experiments have provided a considerable insight in the understanding of the anomalous properties of high T_c-superconductors. Neutron measurements have shown the persistence of antiferromagnetic (AF) dynamical correlations over the whole metallic state of cuprates[1] which demonstrates the strong electronic correlations existing in metallic cuprates. Together with the nuclear magnetic resonance (NMR)[2, 3] and later with bulk magnetic susceptibility[4], INS has evidenced the "spin pseudogap" phenomenon in underdoped cuprates, a topic of intense current interest. Further, INS has shown that these spin excitations are very intimately linked to superconductivity as a sharp magnetic peak occurs when entering the superconducting state. This peak, referred to "resonance" since its first evidence by J. Rossat-Mignod *et al*[5], has spawned a considerable theoritical activity.

The structural peculiarity of high-T_c cuprates is that they are all built from stacking of CuO_2 planes separated by different kinds of layers, the "charge reservoirs", which are essential as they control the charge transfer mechanism. The CuO_2 plane is of central importance as it carries most of the anomalous physical properties in the normal state and, likely, contains the keypoint for the mechanism of high-T_c superconductivity as it has been proposed in many different approaches (See e.g. [6, 7, 8, 9, 10, 11]). The unusual properties of high-T_c cuprates are extensively reviewed in this book and will not be discussed here in details.

A generic phase diagram, sketched in Fig. 1, has been established on phenomenological grounds. Starting from an insulating and antiferromagnetically ordered state around zero doping with one electron per Cu $d_{x^2-y^2}$-orbital, the cuprates become metallic by introducing holes (or electrons) from the charge reservoirs to the CuO_2 plane.

The Gap Symmetry and Fluctuations in High - T_c Superconductors
Edited by Bok *el at*., Plenum Press. New York, 1998

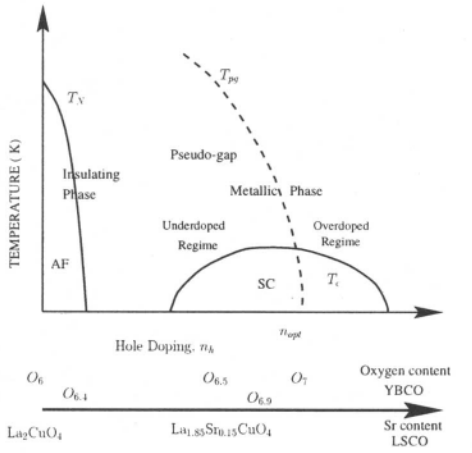

Figure 1: Schematic phase diagram of high-T_c cuprates. The dashed line corresponds to a crossover temperature, T_{pg}, below which most physical properties exhibit or infer a pseudogap behavior. Real systems are indicated versus hole doping in the bottom part. Note that T_N in YBCO disappears for $x \sim 0.4$ which actually corresponds to only about 2-4% of holes in each CuO_2 plane[1].

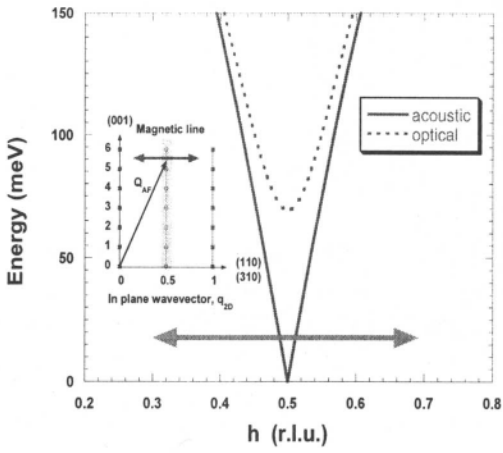

Figure 2: Spin-wave dispersion along the (110) direction in undoped YBCO. Inset displays the scattering plane in the reciprocal space commonly used in INS measurements with $Q = (h, h, q_l)$ or $Q = (3h, h, q_l)$. Squares represents nuclear Bragg peaks and circles AF Bragg peaks occuring in the Néel state. The two arrows indicate a typical Q-scan trajectory performed across the magnetic line.

A superconducting (SC) phase occurs at further doping defining an optimal doping, n_{opt} when the superconducting transition, T_c, is passing through a maximum. Doping rates, below and above n_{opt} define usually called underdoped and overdoped regimes, respectively. In the underdoped state, many physical properties exhibit anomalous behavior below a crossover temperature, T_{pg}: that is the case for the macroscopic spin susceptibility, NMR Knight shift, specific heat, transport properties[4]... In that doping range, it has been shown by NMR[2, 3] and INS[1, 5] experiments that the spin fluctuations are charaterized at low temperature by the opening of a spin pseudo-gap. Recently, photoemission experiments[12, 13] have evidenced that the single-particle excitation spectrum exhibits also a pseudo-gap in the normal state below T_{pg}. Similar observations have been done in optical conductivity[14] and Raman scattering[15] measurements. Concomitantly, these pseudo-gap observations disappear above the optimal doping. Few attempts have been made to describe the phase diagram which have raised questions such as: do the antiferromagnetic fluctuations alone explain the observed phases[6, 7, 8], or, do we need to consider a new critical point at optimal doping which would scale the physical properties[16] as proposed, for instance, in the "circulating current" phase[11] ? Conversely, a comprehensive microscopic description of all these gap observations is still missing at present.

Here, it is important to relate this generic phase diagram of cuprates to the phase diagram of the two systems on which INS experiments have been performed so far. In particular, in $YBa_2Cu_3O_{6+x}$ (YBCO) system, the relation between hole doping, n_h, and oxygen content is not obvious due to the charge transfer mechanism from the Cu-O chains to the CuO_2 planes[17]. Oxygen concentrations from $x \simeq 0$ to $x \simeq 1$ cover a major part of the phase diagram and are reported on Fig. 1 for typical doping regimes which will be discussed here: the optimal doping being realized for $x = 0.94$. In the

$La_{2-x}Sr_xCuO_4$ (LSCO) system, maximum T_c is reached for $x = 0.15$ and is generally assumed to match the optimal doping. A close inspection of the neutron results rather suggest that it could correspond to an underdoped regime. The superconductivity could be simply reduced at further doping because of the proximity of structural instabilities.

Furthermore, considering the unusual properties of these materials, one needs to know which kind of magnetism is observed in INS experiments: do we observe spin dynamics associated with the localized copper spins or rather related to the itinerant quasiparticles ? These different hypotheses have been widely addressed in the literature. As a limiting case, the slightly-overdoped $YBCO_7$ ($x \simeq 1$) could likely be described as a simple itinerant magnetism since, as expected for usual metals, antiferromagnetic spin fluctuations are practically not sizeable in the normal state[18, 19]. Unfortunately, this simple Fermi liquid approach fails at lower doping since dynamical AF correlations are unambiguously observed up to the optimal doping. One then needs to take into account the underlying antiferromagnetic background. Furthermore, the anomalous spectral lineshape detected in photoemission experiments[12] exhibits a behavior inconsistent with conventional band theory indicating that the single-particle spectra are necessarily renormalized due to electron-electron interactions. These "dressed" quasiparticles could even be strongly coupled to collective excitations centered at the AF momentum[20, 21], namely the spin fluctuations. The determination of the energy, momentum, doping and temperature dependences of the spin excitation spectrum is then of primarily importance to describe the anomalous properties of these materials.

Going from well-defined magnons (in the Néel undoped state) related to the localized copper spins to a Fermi liquid picture (at the highest doping available), INS experiments cover a whole range of situations where the spin and charge responses are intimately linked. More generally, INS observations provide direct information about the electronic interactions within CuO_2 planes, and even, between the two adjacent metallic CuO_2 layers in YBCO. Here, I shall review the doping evolution of the spin dynamics. After a short recall of the neutron technique (Sec. 2) and of the experimental difficulties (Sec. 3), magnons in the AF state are reported in Sec. 4. The momentum and energy dependences in the metallic state are presented in Sec. 5 and 6, respectively. The strong modifications of the spin dynamics induced by superconductivity are discussed in Sec. 7. The normal state spin susceptibility, characterized by a "spin pseudogap", is emphasized in Sec. 8. Most of the results described here concerns the YBCO system although comparisons with the LSCO system are occasionally made.

2. INELASTIC NEUTRON SCATTERING

The interaction of neutrons with the condensed matter is double[22]: nuclear interaction with the atomic nucleus and magnetic dipolar interactions between the neutron spin and magnetic moments in solids, spin of unpaired electrons for instance. Neutron scattering is then a very unique tool as it measures in the same time structural information (as can do X-ray scattering) but also magnetic properties. Furthermore, thermal neutrons which possess a wavelength of the order of the atomic distances, 0.5-10 Å, have in the same time an energy, 0.1 - 200 meV, which covers the large range of excitations in solids. Inelastic neutron scattering then gives invaluable information on both spatial and time-dependent of nuclear (like phonons) and magnetic correlations whose momentum and energy dependences are only accessible using INS. An extensive review of the possibilities of neutron scattering can be found in a recent course[23]. Here, it is worth emphasizing that single crystals are required to determine a complete

momentum dependence of dynamical properties. Also, due to the weak interaction of neutrons with condensed matter, neutron scattering probes samples in bulk, but conversely requires large samples.

In high-T_c cuprates, INS using the triple-axis spectrometer technique[23] has been widely used to study phonons[24]. Here, we focus on magnetic scattering whose cross section is directly proportional to the scattering function which is identified to the Fourier transform in time and space of the spin-spin correlation function[22] as,

$$S^{\alpha\beta}(Q,\omega) = \frac{1}{2\pi\hbar}\int_{-\infty}^{+\infty} dt \exp(-i\omega t) < S^{\alpha}_{Q} S^{\beta}_{-Q}(t) > . \qquad (1)$$

This scattering function is in turn related to the imaginary part of the dynamical generalized spin susceptibility, $Im\chi(Q,\omega)$, by the fluctuation-dissipation theorem. Here, we consider a single component of the dynamical generalized susceptibility tensor associated with Carthesian spin coordinates S^{α} and S^{β} with $\alpha, \beta = x, y, z$,

$$\chi^{\alpha\beta}(q,\omega) = -(g\mu_B)^2 \frac{i}{\hbar}\int_{0}^{\infty} dt \exp^{-i\omega t} < [S^{\alpha}_{Q}(t), S^{\beta}_{-Q}] > . \qquad (2)$$

In isotropic magnetic systems, χ is simply identified to $\mathrm{Tr}(\chi^{\alpha\beta})/3$. $Im\chi(Q,\omega)$ is a very useful quantity, especially when no theory can be used to describe the data. It basically contains all the physical interest and can be calculated in different microscopic models. In undoped Néel state, the spin susceptibility describes the excited states above the AF ground state, referred to as magnons[22], and neutron scattering cross-sections are well described using spin-wave theory in Heisenberg model. When adding a small amount of holes in CuO_2 planes ($n_h \leq 5\%$), the system remains in the insulating state, but very peculiar spin dynamics is observed: the low energy excitations are strongly enhanced at low temperature[25, 26, 27] likely due to electron-hole interactions. Increasing further the doping, spin fluctuations are still detected in the metallic state. Further, by calibration with phonon scattering, INS experiments provide absolute units for the dynamical susceptibility which are important for theoritical models. This absolute unit calibration is also necessary to compare the INS results in different systems as well as results obtained using different techniques (with NMR measurements for instance).

In undoped cuprates, the ordered AF phase is characterized by an in-plane propagation wave vector, $q_{AF} = (\frac{1}{2}, \frac{1}{2}, 0)$ and the magnetic neutron cross section is maximum at wave vectors like $\mathbf{Q} = \tau + \mathbf{q_{AF}}$, where τ denotes Bragg peaks of the nuclear structure (squares in the inset of Fig. 2). Roughly speaking, when going into the metallic state, the magnetic scattering remains always peaked around the in-plane component of the AF wave vector. This occurs for any values of the momentum transfer q_l perpendicular to the plane. The magnetic scattering is then concentrated around lines in the reciprocal lattice, like $(\frac{h}{2}, \frac{k}{2}, q_l)$ with h and k integers, denoted magnetic lines. Q-scans, performed within a Brillouin zone across these lines and at different energy transfers (sketched by the arrow in Fig. 2), exhibit a maximun around $q_{AF} \equiv (\pi, \pi)$ (Fig. 3) which is likely identified to the magnetic scattering.

3. EXPERIMENTAL EVIDENCE OF MAGNETIC EXCITATIONS

Unfortunately, INS experiments are not only measuring the magnetic scattering: other contributions occur either due to intrinsic nuclear scattering of the lattice, like phonons, or even due to spurious effects and impurities. Furthermore, owing to the

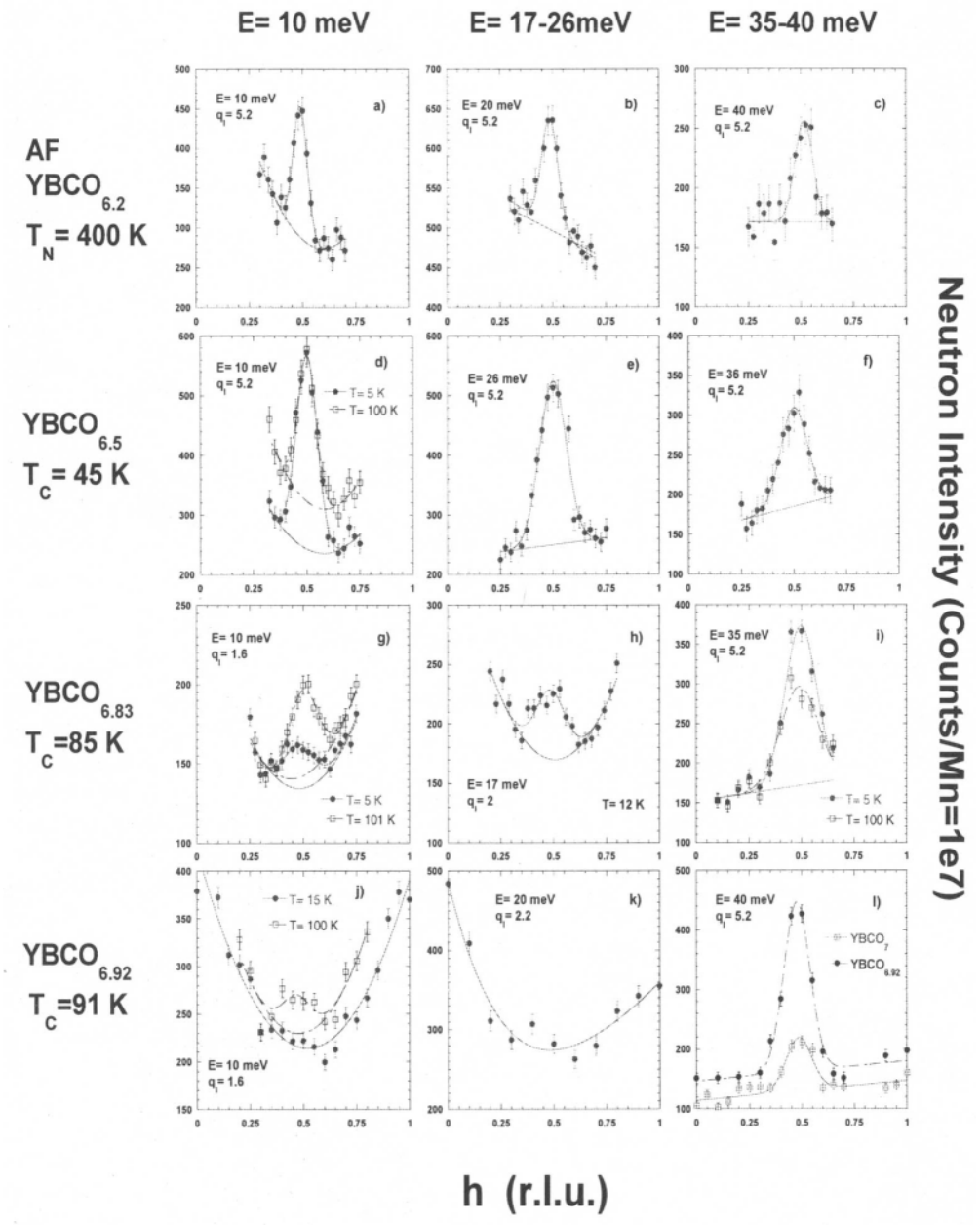

Figure 3: Q-scans performed across the magnetic line, $Q = (h, h, q_l)$, where h is scanning over two Brillouin zones. All neutron intensities are normalized to the same units, and are then directly comparable each others. The *qi* value along the (001) direction was chosen to get the maximum of the magnetic structure factor[1]. In the AF state $(x = 0.2)$, only a single peak is observed for the counterpropagating spin-waves; this is caused by resolution effect of the spectrometer. Note the strong reduction of the E= 40 meV peak intensity from $YBCO_{6.92}$ (nearly optimally doped regime) to $YBCO_7$ (overdoped regime) (Fig. 3.1).

relatively weak cross section of the magnetic scattering, its extraction from the total scattering is a major experimental problem encountered in INS experiments. In principle, polarized neutron beam experiments should easily separate these contributions, the magnetic scattering appearing in the spin-flip channel at the difference of nuclear scattering. However, due to the lack of statistics, polarized neutron results have yielded partly erroneous conclusions in high-T_c cuprates [28]. Therefore, unpolarized neutron experiments have been largely employed. Due to the experimental difficulty, new results always need to be crosschecked and confirmed by other measurements because a single isolated experiment can be unfortunately misled by spurious effects. It has led to extensive, sometimes contradictory, discussions over the last decade[1, 18, 19, 28, 29, 30, 31, 32]. *Only* the use of complementary methods as well as the accumulation of neutron data allow to overcome the experimental difficulties. Here, I shall briefly recall the main guidelines which have been used to estimate the magnetic signal.

Among these methods, let us emphasize the use of the momentum and temperature dependences because they are different for magnetism and phonons[22]. Especially, as a result of the magnetic form factor, magnetic scattering is known to decrease on increasing the amplitude of the wave vector over few Brillouin zones in contrast to the phonon scattering. Within a single Brillouin zone, one could also discriminate both signals by their q-dependences. Further, INS experiments have been also performed in different scattering planes to avoid some specific phonons[19].

Another powerful method developed for the YBCO system has been to conduct experiments in the different regimes of the phase diagram *on the same sample*[1, 30, 32]. Indeed, the $YBa_2Cu_3O_{6+x}$ system offers the great opportunity to cover the whole high-T_c cuprates phase diagram just by changing the oxygen content by thermogravimetry from the Néel state, $x \simeq 0$, to the overdoped metallic, $x \simeq 1$. Measurements scanning the wave vector along the (110) direction are shown in Fig. 3 at few different fixed energy transfers for few different states of YBCO. Further, these experiments have been performed on the same triple axis spectrometer (2T-Saclay) using the same experimental setup, i.e. the same spectrometer resolution. This gives the great advantage that impurity contributions and, in a less extent, the phonons are basically the same in all experiments: this facilitates the extraction of the magnetic scattering.

These scans exhibit at any doping well-defined maxima at $q = 0.5$, corresponding to the AF wave vector $\equiv (\pi, \pi)$, whose magnitude evolves with doping. At $E = 10$ meV, a correlated scattering signal is seen at lower doping whereas it is absent for optimally doped samples. In contrast, the correlated signal at $E = 40$ meV first increases with the oxygen content and then decreases for $x \simeq 1$. Measurements at nearly the same energy in the normal state exhibit, at most, a very weak magnetic signal (see Fig 11). These striking doping, energy and temperature dependences have given strong guidelines to analyse the data. In particular, two clear limits are well-defined: the undoped case where the theoritical spin-wave cross section is known and the case of the normal state in the overdoped regime where the very weak magnetic scattering can be neglected. A generic shape for the non-magnetic contributions is then deduced for any doping. The use of such empirical methods, as well as phonon calculations[33], give a self-consistent picture which has made possible to improve the data analysis all over the years[1, 5, 30, 32]. When using the triple-axis technique, a good confidence is now reached about the determination of the magnetic signal over a wide range of energy [34, 35]. However, it should be mentioned that this method excludes contributions which are weakly momentum-dependent. Unfortunately, no current neutron experiment is able to evidence such hypothetic magnetic contributions.

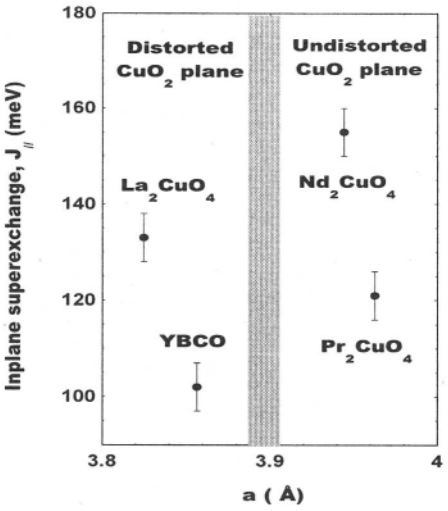

Figure 4: In-plane superexchange interaction determined by INS experiments versus Cu-Cu distance in different cuprates (from [38]).

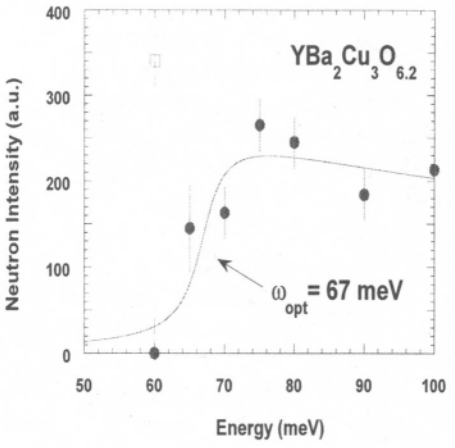

Figure 5: Energy dependence of the neutron intensity at q_{AF} from spin-wave scattering at T=10 K (from [40]). The closed (open) symbols represent the intensity of the optical (acoustic) excitations. The full line is a fit by a step-like function.

4. ANTIFERROMAGNETIC STATE AND EXCHANGE PARAMETERS

Undoped parent compounds of high-T_c cuprates are Mott-Hubbard insulators which are usually described by a spin-$\frac{1}{2}$ antiferromagnetic Heisenberg model on a square lattice[36]. They exhibit an antiferromagnetic ordering below a Néel temperature ranging between 250 K and 420 K[1]. The most important parameter is the Cu-O-Cu nearest neighbor superexchange interaction, J, within the CuO_2 plane.

In ordered magnetic systems, INS experiments probe the spin-wave dispersion relations which relate the magnon energy, ω_q, to the scatterred wave vector (see Fig. 2). At sufficiently low energy (but notably above the small magnon gaps related to interlayer coupling and exchange anisotropies[1, 37]), the acoustic magnon dispersion relation starts linearly in AF systems as $\omega_q = cq$ (Fig- 2). J is then deduced from the measured spin-wave velocity c, as $c = 2S\sqrt{2}Z_c Ja$ (where a is the square lattice constant, S=$\frac{1}{2}$ and $Z_c \simeq 1.18$ represents quantum corrections of the AF ground state). Unfortunately, because of the large value of J and of resolution effect, counterpropagating spin-waves cannot be observed when scanning across the magnetic line (as sketched in Fig. 2): a single peak is usually measured (see Fig 3a-c). A special scattering geometry has thus been adapted to determine the spin-velocity with accuracy in $YBa_2Cu_3O_{6.1}$[37] and in three different monolayer undoped cuprates(La_2CuO_4, Nd_2CuO_4 and Pr_2CuO_4) [38]. The deduced in-plane antiferromagnetic superexchange coupling J is typically 130 meV (Fig. 4). However, J does not exhibit a monotonous behavior versus the bonding Cu-O-Cu length likely on account of detailed structure of each system. It underlines that the large enhancement of J is caused by other structural units like the Cu-0-0 triangle[39].

Further, the unit cell of YBCO contains pairs of closely spaced CuO_2 layers, the bilayers. The intrabilayer coupling, referred as $J_\perp$, removes the degeneracy between even- and odd-parity electronic states. In the AF Néel state, these excitations correspond to optical (dashed line in Fig. 2) and acoustic (full line in Fig. 2) spin waves, respec-

tively. These two modes display complementary dynamical structure factors along the momentum transfer perpendicular to the basal plane, q_l: $\sin^2(\pi z q_l)$ for the acoustic mode and $\cos^2(\pi z q_l)$ for the optical mode. (Here, $z = 0.29$ is the reduced distance between nearest-neighbor Cu spins within one bilayer). This allowed to distinguish these two excitations and to determine the optical gap[40, 41]. Fig. 5 show the energy dependence of the neutron intensity at q_{AF} obtained from our results[40] which gives an optical magnon gap at $\omega_{opt} = 67 \pm 5$ meV. Hayden *et al*[41] have reported a slightly larger value from less accurate data. Detailed spin-wave calculations[1, 37] reveal an optical magnon gap at[40], $\omega_{opt} = 2\sqrt{J_\perp J}$. Using the value of $J = 120$ meV[37, 41] for the in-plane superexchange, one deduces $J_\perp = 9.6$ meV. However, the above relation does not account from quantum corrections of the AF ground state. A more accurate treatment using Schwinger bosons representations[42], gives $J_\perp \sim 12$ meV which is in good agreement with band theory predictions[43], $J_\perp \sim 13$ meV. In classical superexchange magnetic theory, where J is proportional to the square of the overlap of the electronic wavefunctions, one can deduce the ratio between the intrabilayer and the inplane hopping matrix elements as $\frac{t_\perp}{t} = \sqrt{\frac{J_\perp}{J}} = 0.34$. This non-negligible ratio, which unlikely would vary with doping, shows that the electron transfer processes between direcly adjacent layers could play an important role in the high-T_c mechanism as it was suggested in the interlayer tunneling model[44].

Furthermore, by calibration with phonon cross section, one can determine the spectral weight of the spin susceptibility in absolute units. Surprisingly, the spin wave spectral weight is found smaller than expected from quantum corrections[38]. This reduction of about 30% is presumably due to covalent effects between copper d-orbitals and oxygen p-orbitals[45]. Reducing the absolute scale of the atomic form factor, such effects can also explain the reduction of the low temperature ordered magnetization value[1, 45].

5. WAVE VECTOR DEPENDENCES IN THE METALLIC STATE

We now turn to the results in the metallic state of cuprates where the magnetic scattering is only found inelastic, corresponding to dynamical fluctuations and peaked around the AF wave vector. The existence of these fluctuations is already surprising since in usual simple metals fluctuations arising from free electrons are too weak to be observed. This observation then signs the existence of strong electronic correlations in high-T_c cuprates.

Even and Odd excitations in YBCO: q_l-modulation in YBCO

In conventional band theory, interactions within a CuO_2-bilayer yield bonding and antibonding bands in the metallic state. Transitions between electronic states of the same type (bonding-to-bonding or antibonding-to-antibonding) and those of opposite types are characterized by even or odd symmetry, respectively, under exchange of two adjacent CuO_2 layers. As a result, odd and even excitations then exhibit a structure factor along q_l similar to the acoustic and optical spin-wave in the Néel state, respectively. As discussed in the previous section, this yields a $\sin^2$-type q_l-dependence of the lower energy excitations, the odd excitations. This structure factor has been effectively observed in any low energy (below ~ 45 meV) magnetic studies. It is, for instance, the case in Fig. 6 in the SC state of optimally doped YBCO. Similar results have been reported in the normal state as well[1, 46, 47]. In weakly

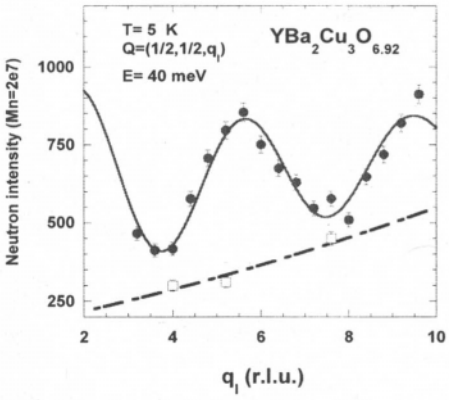

Figure 6: q_l-scan at E = 40 meV in $YBCO_{6.92}$ displaying a modulation typical of odd excitation (from [1]). The background, obtained from q-scans across the magnetic line (open squares), is represented by the dashed line. The full line correspond to a fit by $a+bF^2(Q)\sin^2(\pi z q_l)$ above the background and where $F(Q)$ is the Cu magnetic form factor.

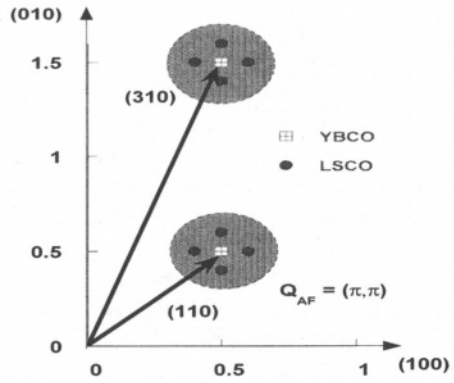

Figure 7: In-plane Brillouin zone. The shaded area sketches the location of AF fluctuations. The closed circles sketch the four-peaks magnetic scattering observed at low energy in the LSCO system at $Q = (\pi(1 \pm \delta), \pi)$ and $Q = (\pi, \pi(1 \pm \delta))$, displaced from the AF momentum by an amount, $\delta = 0.245 = 0.28$ Å^{-1} for $x = 0.14$[50].

doped metallic state, $x \sim 0.5$, this modulation actually occurs because even excitations exhibit a gap around 53 meV[34], which is reminiscent of the optical magnon gap[40]. At higher doping, the even excitations gap is lowered further by doping (~ 35 meV in $x \simeq 0.7$)[35]. Surprisingly, the $\sin^2$-structure factor is still observed at energies above this even gap (Fig. 6). However, Fig. 6 suggests that this modulation is not complete as even excitations are sizeable at $q_l \simeq 3.5, 7$ but with a magnitude ~ 5 times smaller. Therefore, although the even excitations occur in the same energy range, they are surprisingly much weaker in amplitude than the odd excitations. Moreover, even excitations display unexpected temperature dependences[34, 35] as they are strongly reduced going fom 5 K to 200 K.

Commensurate fluctuations in YBCO

We then discuss the in-plane wave vector dependence observed at low energy results, i.e. below $E \sim 40$ meV. As shown in Fig. 3, the magnetic scattering is found in YBCO peaked at the AF momentum, (π, π), at any doping. However, it has been recently reported[48] that the magnetic fluctuations in an underdoped $YBCO_{6.6}$ (T_c = 63 K) sample would become incommensurate around $E \sim 25$ meV, but only below $T \sim$ 70 K. This contradictory result needs to be confirmed as only a few measurements[49] have previously indicated, at most, a flat-topped shape of low-energy q-scans profiles. In any case, typical observed peaks are far from simple sharp Lorentzian-shape peaks. As shown for instance at E = 17 meV in $YBCO_{6.83}$ in Fig. 3h, two broad peaks could better described the observed profile. Actually, the extension in q-space of the magnetic scattering is quite important as its q-width, defined as the Full Width at Half Maximun (FWHM) Δ_q, is typically about one fifth of the Brillouin zone size. On increasing doping, the peak broadens (see Fig. 3), giving at most $\Delta_q \simeq 0.45$ Å^{-1}[30, 32] (after resolution deconvolution when fitting by a Gaussian shape) for highly doped samples,

$x \geq 0.9$ whereas $\Delta_q \sim 0.25$ Å^{-1} is found for weakly doped samples, $x \sim 0.5$. This q-width may be associated with a length in real space, $\xi = 2/\Delta_q$, which would correspond to an AF correlation length in a localized spins picture. Typically, this length is found very short[30], as $\xi/a \sim 1 - 2.5$ depending on doping (where a=3.85 Å). Furthermore, Δ_q, still obtained by a Gaussian fitting of the q-lineshape, displays no temperature dependence within error bars (see e.g. [32]).

Incommensurate fluctuations in LSCO

In LSCO, the low energy fluctuations clearly differ from what is observed in YBCO: a four-peaks structure is observed[50, 51] instead of a broad peak centered at (π, π) (Fig. 7). Each spin scattering peak occurs at an incommensurate wave vector which increases with doping. It exhibits a q-width much smaller than in YBCO such as the four peaks do not overlap. On increasing energy, the peaks broaden and concomitantly the incommensurability disappears: the spin scattering being maximum at (π, π) with a large q-width for energies above ~ 25 meV for $x = 0.15$[51].

The origin of the incommensurability in LSCO has been widely discussed in the framework of itinerant magnetism[52, 53, 54, 55]. Magnetic correlations are enhanced at the incommensurate wave vectors due to a near nesting property of the simple bidimensional Fermi surface deduced from simple tight-binding calculations. At the AF wave vector, low energy spin fluctuations are removed up to an energy which is twice the chemical potential[55]. This picture seems to nicely account for the observed features. However, the calculation of the chemical potential from the doping level cannot be deduced from conventional band structure calculations[54] and would be associated with new quasi-particles charge carriers[9]. This model can also explain why the LSCO and YBCO systems display different momentum dependences according to a different Fermi surface topology in the two systems[52, 53]. However, quite recently, another interpretation, based on real-space domains observed in insulating phases caused by charge ordering forming stripes[56], has been proposed to explain the discommensuration[57].

6. ENERGY DEPENDENCE OF THE SPIN SUSCEPTIBILITY

The most remarkable INS result in high-T_c cuprates is certainly the drastic change of the spin dynamics when entering the superconducting state. Basically, a gap opens at low energy, E_G, and a strong resonance peak appears in the odd spin susceptibility at a characteristic energy, E_r. These features are most likely related to coherence effects because of spin pairing of the superconducting electron pairs as it has been inferred in conventional BCS formalism[58]. However, the observed characteristics imply unconventional superconducting gap symmetry, i.e. anisotropic gap in **k**-space, most probably of d-wave symmetry. These features as well as their implications are described in the two next sections. The normal state properties will be discussed in a third section.

Doping dependence of the odd spin susceptibility and resonance peak

In order to emphasize these features, it is convenient to discuss the energy shape of the odd spin susceptibility. Fig. 8 depicts $Im\chi$ in the superconducting state for energies below 50 meV and at the AF wave vector: $Im\chi$ is displayed for 6 different oxygen contents, 4 in the underdoped regime and 2 in the overdoped regime. The

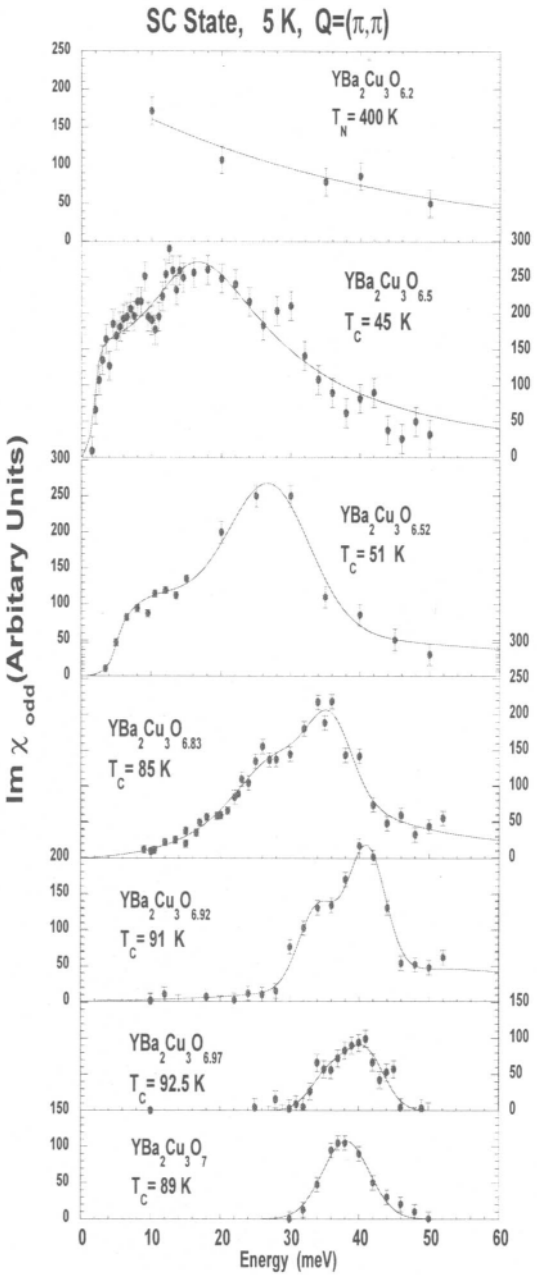

Figure 8: Imaginary part of the odd spin susceptibility at T= 5 K in the superconducting state for six oxygen contents in YBCO. At the top, the spin waves scattering of the undoped parent compound at T=8 K is displayed for comparison. (See Fig. 9 for other details).

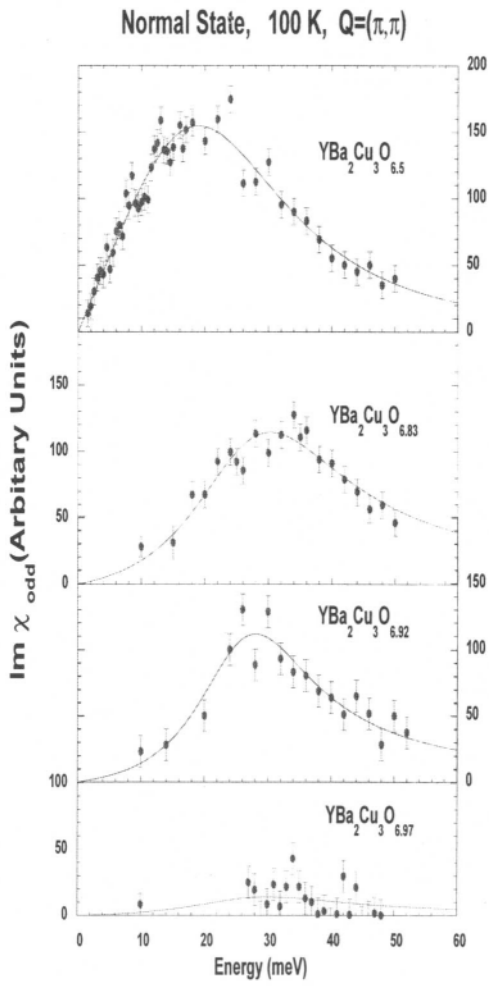

Figure 9: Imaginary part of the odd spin susceptibility at T= 100 K in the normal state for four oxygen contents in YBCO. These curves are directly comparable each others from measurements performed on the same triple axis spectrometer (2T-Saclay). They have been normalized to the same units using standard phonon calibration [33]. Using further measurements[34], 100 counts in the vertical scale would roughly correspond to $\chi_{max} \sim 350\ \mu_B^2/\mathrm{eV}$ in absolute units.These curves are in the same units as those of Fig. 8. Lines are fit by Eq. 6.

normal state (T= 100 K) spin susceptibility is reported on Fig. 9 for four different samples equivalent to those reported in the SC state: 3 in the underdoped regime, 1 in the overdoped regime. All these measurements have been scaled to the same units from an analysis as discussed in section 3. The results have been obtained on the same sample, except for the $x = 0.97$ sample[18] which have been scaled using phonon calibration.

One first clearly notices that $Im\chi$ strongly evolves with doping. $Im\chi$ is characterized by a maximum which becomes sharper in energy for higher doping. In addition to that peak, magnetic correlations occur at other energies. For instance, the spin response in the nearly optimally case $YBCO_{6.92}$ displays a strong resolution-limited peak located at 41 meV and a plateau in the range 30-37 meV. Normal state AF fluctuations exist in a wider energy range with a broad maximum around 30 meV. The 41 meV enhancement has totally vanished at T= 100 K and has been, therefore, assigned to a "magnetic resonance peak", E_r[5].

Upon increasing doping, the resonance peak is slighly renormalized to lower energies whereas the plateau is substantially removed, so that, the SC spin susceptibility is basically well accounted for by a single sharp peak around E_r= 39-40 meV for fully oxidized $YBCO_7$ samples. A clear agreement is now established among the neutron community about this slightly overdoped regime [18, 19, 29, 32]. The most important result is that this resonance peak intensity disappears at T_c as shown in Fig. 10. Performing a q-scan at the resonance energy in both the SC state and in the normal state emphasizes the vanishing of the resonance peak above T_c: Fig. 11 displays a q-scan at $\hbar\omega = 39$ meV with very weak magnetic intensity at (π, π) and T= 125 K[47]. This striking temperature dependence demonstrates that this peak is intimately related to the establishement of superconductivity. Fig. 10 shows that the resonance intensity actually follows an order parameter-like behavior[5, 18, 29, 33] whereas the resonance energy is itself very weakly temperature dependent, if any[18, 28, 33]. The q-scan at 39 meV also underlines the strong reduction of the normal state AF correlations in the overdoped regime. This is in sharp contrast with the nearly optimally doped sample, $YBCO_{6.92}$[32]: on a more quantitative ground, Fig. 9 reveals that the AF correlations amplitude is reduced at T=100 K by a factor ~ 2-4 (depending of the energy) going from $x = 0.92$ to $x = 1$.

On lowering doping, the spin susceptibility spreads out over a wide energy range. However, a close inspection of **q**- and temperature dependences of $Im\chi$ reveals that the resonance peak feature is still present in underdoped samples[30, 31, 32]. This can be demonstrated by making the difference between the neutron intensity measured at T= 5 K at Q=(π, π) and the same scan measured just above T_c[28, 59]: this difference exhibits a sharp peak at energy where $Im\chi$ at T=5 K is maximum. Here, the whole lineshape of $Im\chi$ is preferably reported as it can be directly compared with theoritical models. The resonance peak energy is shifted to lower energy in underdoped regime, actually following T_c[31, 59] (Fig. 12). The relative amplitude of the resonance peak as compared to the normal state intensity is decreasing with lowering oxygen content, so that, the resonance amplitude is about 50% of the maximum intensity for heavily doped samples ($x \geq 0.6$, $T_c > 60$ K , when the resonance energy is located around ~ 34 meV,)[28, 31, 35], and only about 15% for weakly-doped samples ($x \simeq 0.5$, $T_c \sim 50$ K and $E_r \simeq 25$ meV)[34]. In contrast, the intensity at the maximum at T= 5K actually increases with decreasing doping. Conversely, the normal state excitations is larger in the weakly-doped range (see Fig. 9). Therefore, although the spectral weight of $Im\chi$ becomes larger, the resonance feature vanishes for smaller doping and T_c.

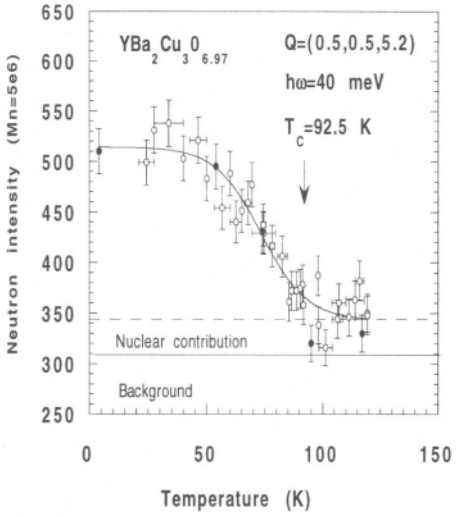

Figure 10: Temperature dependence of the resonance peak at E= 40 meV (from [18]). The reported "nuclear contribution" is due to a phonon peak whose maximum intensity is located at 42.5 meV[19].

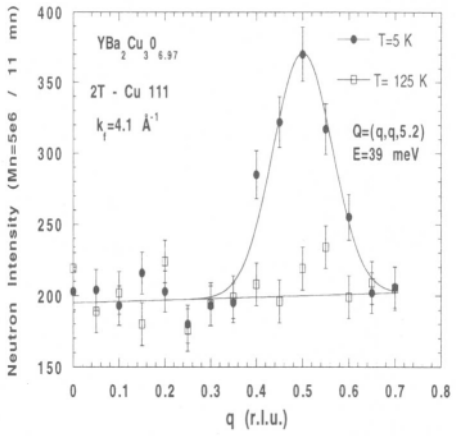

Figure 11: Q-scans across the magnetic line at the resonance energy in the overdoped regime. These data are giving the most accurate upper limit of the normal state AF intensity which is about 8 times smaller than the resonance peak observed in the SC state.

Spin gap in the SC state

In the superconducting state, the spin susceptibility is limited at low energy by a gap below which no AF scattering is visible. This energy gap is then defined by the first inflexion point of $Im\chi$ curve and is referred to as "spin-gap", E_G. Below E_G, q-scans display no or very weak peak at (π, π), as displayed, at 10 meV in Fig. 3g and Fig. 3j. Going into the normal state (T=100 K), the spin-gap is suppressed because low energy excitations are sizeable at (π, π). Moreover, the peak intensity appears on heating at T_c[32] demonstrating that this spin gap is directly related to the superconducting gap. Further, E_G increases upon doping[30] but with a different dependence than the resonance energy.

In most cases, E_G is defined by a sharp resolution-limited step (Fig. 8). However, this low-energy step is found much broader for x = 0.83. Concomitantly, the superconducting transition of this sample was also broader than usual. Therefore, it is reasonable to attribute this behavior to the lack of sample homogeneity which could smear the sharp features of the spin response. Nevertheless, a resonance peak has been clearly observed in that sample[30] whose relative amplitude might be only reduced as compared with subsequent reports[28, 31, 59].

This comparison between spin-gap and T_C-width also gives some insight about two related issues. First, in the weakly-doped $YBCO_{6.5}$ regimes, this spin-gap has been widely reported by the french group[1, 5, 30, 32] and not by others[60] for sample having similar oxygen contents and T_c. As a matter of fact, a close inspection of the T_c-curves reveals that the samples exhibiting a spin-gap had clearly a sharper SC transition. Second, it may solve a controversy existing in LSCO system where a spin-gap has been reported only recently[51, 61]. Previous studies have not succeeded to detect it[50] likely because of sample inhomogeneities and/or impurity effects. More generally, the observation of the spin-gap appears to be very sensitive to sample defects

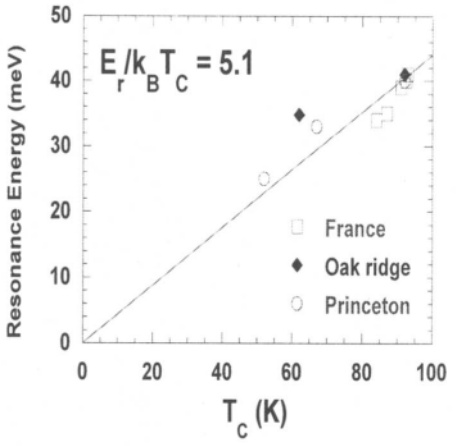

Figure 12: Resonance energy in YBCO versus T_c. French results are from [18, 30, 31, 32], Princeton results are from [19, 59], Oak Ridge results are from [28, 29].

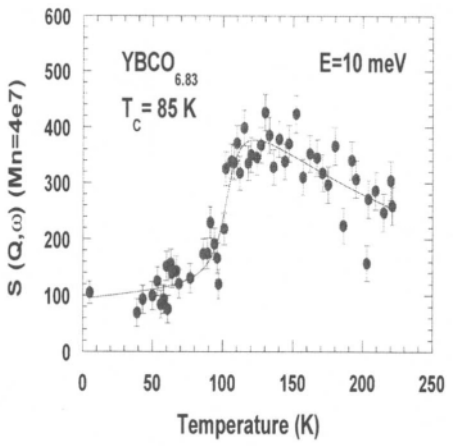

Figure 13: Temperature dependence of the peak intensity at low energy in $YBCO_{6.83}$. Background has been subtracted using q-scans (see Fig. 3).

and impurities. As an example, the controlled substitution of 2% of zinc in overdoped YBCO (where T_c is reduced by ~ 20 K) induces low energy AF fluctuations below the spin-gap[26, 62].

Finally, it is very interesting to draw a parallel between the spin response in superconducting state of LSCO near maximum T_C (x = 0.14) and in weakly-doped underdoped $YBCO_{6.5}$. Both systems display a small spin gap in the SC state of about 2-5 meV. Both systems also exhibit a subtle enhancement of the spin susceptibility just above the spin gap: in LSCO, it has been underlined[63] that around 9 meV an additional enhancement occurs only in the SC state which is accompanied to a sharpening in momentum space. Similar observations have been previously reported around 7 meV in $YBCO_{6.52}$[64]. In light of the recent experiments in $YBCO_{6.5}$[59], it seems that this effect is different from the resonance peak feature occuring at higher energy. However, this issue is still under debate as no resonance peak has been detected so far in LSCO. Besides, this could be simply because the resonance intensity is expected to be only ~ 10 % of the total magnetic scattering for such low $T_c \leq 40$ K, still by comparison with $YBCO_{6.5}$[34].

7. COHERENCE EFFECTS IN THE SUPERCONDUCTING STATE

As the resonance peak and the spin-gap are both intimitaly related to the superconductivity, a simple interpretation has then been proposed in itinerant magnetism approaches[42, 65, 66, 67, 68, 69, 70, 71, 72]. Beyond different hypotheses, these models basically show that the resonance peak occurs simply because of the BCS pairing. Starting from a Fermi liquid picture, the non-interacting electronic spin susceptibility (Lindhard Function) is written as,

$$Im\chi^{\circ}(q,\omega) = (g\mu_B)^2 \lim_{\epsilon \to 0} \sum_k \frac{f_{q+k} - f_k}{\epsilon_{q+k} - \epsilon_k - \hbar\omega - i\epsilon} \qquad (3)$$

where ϵ_k is the electronic band dispersion and f_k is the associated Fermi function.

This spin susceptibility is described by the two-particle response function which usually gives featureless broad response due to sum over the reciprocal space. However, band structure singularities and nesting effects can induce rather complex lineshapes and q-dependences. Going into the SC state, one should account for the spin pairing of Cooper pairs[58], $Im\chi^{\circ}$ then becomes for T=0,

$$Im\chi^{\circ}(q,\omega) = (g\mu_B)^2 \lim_{\epsilon \to 0} \sum_k \left[1 - \frac{\Delta_k \Delta_{q+k} + \epsilon_{q+k}\epsilon_k}{E_{q+k}E_k}\right] \frac{1 - f_{q+k} - f_k}{E_{q+k} + E_k - \hbar\omega - i\epsilon} \qquad (4)$$

with $E_k = \sqrt{\Delta_k^2 + \epsilon_k^2}$ and Δ_k is the **k**-dependent SC energy gap. The term in brackets is a coherence factor related to the BCS pairing[58]. This function displays a soft edge behavior when the sum $(E_{q+k} + E_k)$ is mimimum[68, 72] but not a sharp peak. Further, the q-dependence of this function is not necessarily peaked around (π, π)[71]. Therefore, neutron data cannot be reproduced in a generic noninteracting electron model. To overcome these difficulties, a Stoner-like factor should be included which is related either to band structure singularities, to spin fluctuations, or even to interlayer pair tunneling effects[72]. In the case of a magnetic exchange, $J(q)$, the interacting spin susceptibility using Random Phase Approximation (RPA), is

$$\chi(q,\omega) = \frac{\chi^{\circ}(q,\omega)}{1 - J(q)\chi^{\circ}(q,\omega)} \qquad (5)$$

The RPA treatment have been held responsible for the sharpness of the peak in both energy and momentum. Using this expression, a sharp peak is obtained above a gap and both are proportional to the SC gap. In the normal state, featureless non interacting spin susceptibility for itinerant carriers is restored. Hence, this result in both the normal state and the SC state agrees with what is measured in the overdoped regime.

In this view, the resonance energy, E_r, closely reflects the amplitude of the SC gap as well as its doping dependence. Experimentally, this prediction is supported as the resonance energy is found to scale with T_c with $E_r/k_BT_c \simeq 5.1$ (Fig. 12). However, the true proportionality of the resonance energy with the maximum SC energy gap, Δ_{SC}^{max}, is not simply 2 as expected in simple BCS theory with an isotropic SC gap. Here, it crucially depends on band structure effect[9]. For the same reason, this relation is even more complex for the spin gap doping dependence[68]. Interestingly, this model requires $d_{x^2-y^2}$-wave symmetry of the SC gap function, Δ_k[65, 66, 67, 68, 69, 70], as a change of sign of $\Delta_k\Delta_{Q_{AF}+k}$ should occur in the coherence factor. However, other subtle scenario can occur[71]. Van-Hove singularities in band structure[67, 69] have been also invoked to play a role in the peak enhancement. As the peak position of the resonance exhibits very little temperature dependence[18, 28, 33], the SC gap should not change with temperature in this framework.

Finally, one can conclude that coherence effects related to the spin pairing seem to account for the marked modifications of the spin susceptibility in the SC state. Moreover, the additional enhancement in the SC state observed $\simeq 7 - 9$ meV[63, 64] can be also explained in this framework: a transfer of the spectral weight from the low energy (below the spin-gap, E_G) to energies just above E_G is indeed expected. In any case, the major limitation of this model is that in the underdoped regime (as well as for optimal doping) one observes another magnetic contribution existing in the SC state and remaining in the normal state. This more complex behavior of the spin susceptibility requires more sophisticated models than simple itinerant hole picture.

A correlated-electron model which is aiming to unify superconductivity and antiferromagnetism[8], has been recently proposed to account for the resonance peak. A particle-particle collective excitation occurs in this model[73], whose matrix element coupling this excitation to the magnetic neutron cross section, vanishes in the normal state, but is nonzero in the superconducting state. In this model, because excitation energy is proportional to the hole doping[73], the resonance energy should increase with the oxygen content. Experimentally, this trend is found up to optimal doping. However, going from $YBCO_{6.9}$ to $YBCO_7$, E_r is rather reduced (Fig. 8) following actually T_c in contrast to the expectation.

8. SPIN PSEUDO-GAP AND QUASI-DISPERSION

As stressed in previous sections, the resonance feature is accompagnied in underdoped and optimally doped regimes by another broad contribution which is rapidly stronger in amplitude at lower doping. The odd spin susceptibility is actually maximum at a characteristic energy, ~ 30 meV (see Fig. 9). This maximum of $Im\chi$, which directly corresponds to the pole of the spin susceptibility, then naturally defines a gap in the spin excitation spectrum. Obviously, this gap can be identified to the well-known "spin pseudo-gap"[2, 5, 32] although its definition is different from previous convention[5].

For the sake of clarity, it is useful to describe the normal state spin susceptibility by a damped Lorenztian function. This expression is usually applied to disordered short range localized spins. It is, for instance, the case of one dimensional magnetic system such as the so-called Haldane gap systems[74], $Im\chi$ is then written,

$$Im\chi(q,\omega) = \frac{\chi_q \ \omega \ \Gamma}{(\omega - \omega_{pg})^2 + \Gamma^2} \tag{6}$$

where ω_{pg} is the characteristic energy corresponding to the pole of the spin susceptibility. Eq. 6 is giving a good description of the normal state spin susceptibility (Fig 9) with $\omega_{pg} \simeq 28$ meV in heavily-doped samples ($x \geq 0.6$). In that doping range, the spin pseudo-gap, ω_{pg}, has no marked doping as well as temperature dependences. In contrast the spin gap, defined in Sec. 6, increases with doping. Therefore, these two gaps clearly differ. However, these two gaps "accidentally" occur in the same energy range yielding complex lineshapes in the SC state. Quite independently of the doping, the excitations display a strong damping with $\Gamma \simeq 12$ meV. As a result, sizeable excitations exist in the normal state down to low energy. This differs from the SC state where the low energy excitations are much more reduced by the spin-gap. Fig. 13 displays the temperature dependence of the magnetic scattering at (π,π) and at $\hbar\omega = 10$ meV for $x = 0.83$. In the SC state, small residual magnetic scattering occurs at this energy for that sample (Fig. 3). Upon heating, the AF fluctuations increase in the normal state passing through a maximum around a temperature T^* ~ 120 K larger than T_c. This temperature behavior reminds of that measured by copper NMR experiments in the underdoped regime[2, 3] where the spin-lattice relaxation rate $^{63}T_1$ is related to the spin susceptibility by $1/^{63}T_1T \propto \sum_q Im\chi(q,\omega)/\omega$. Similarly to Fig. 13, $1/^{63}T_1T$ displays a maximum at a temperature T^* in underdoped cuprates. This result has been widely interpreted by the opening of a spin pseudo-gap at the AF wave vector below T^*[2, 3]. More probably, this unusual temperature behavior as well as the value of T^* rather results from the interplay of the magnetic parameters, namely ω_{pg}, Γ and χ_q, which have different temperature dependences.

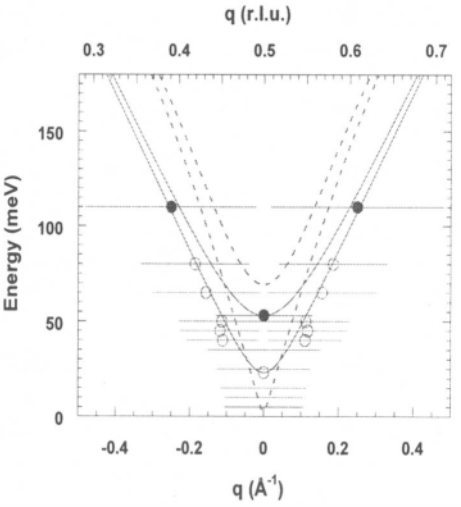

Figure 14: Spin excitation spectrum for odd - "acoustic" - (open circles) and even - "optical" - (closed circles) excitations at 5 K in $YBCO_{6.5}$ (from [34]). The lowest open circle represents the energy of the maximum of the odd susceptibility. The horizontal bars represent the intrinsic q-width (FWHM) after a Gaussian deconvolution from the spectrometer resolution. Full lines correspond to an heuristic quadratic fit like $\omega^2 = \omega_0^2 + c^2q^2$. Dashed lines represent the magnon dispersion curves of the undoped materials.

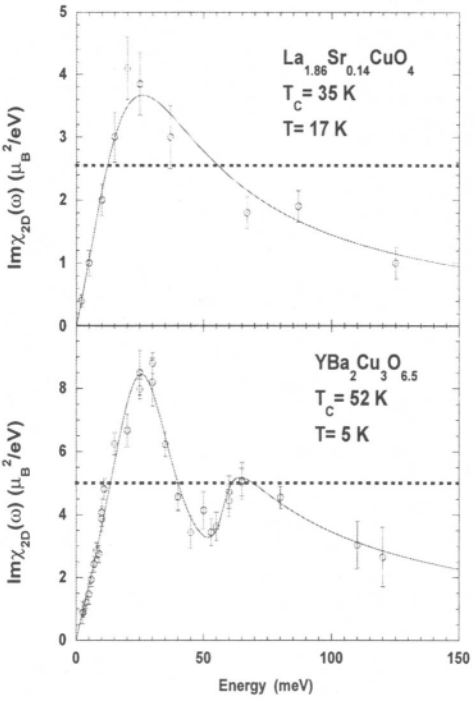

Figure 15: Comparison of the q-integrated spin susceptibility per CuO_2 plane in $YBCO_{6.5}$[34] and in $La_{1.86}Sr_{0.14}CuO_4$[75]. The dashed lines represent the 2D-integrated AF spin-wave contribution which is nearly constant in such an energy range (see[34, 38] for details).

In weakly-doped samples, $YBCO_{6.5}$, ω_{pg} is located ~ 20 meV at T= 100 K (Fig. 9); ω_{pg} is also temperature dependent[32, 34] reaching 30 meV for $T \geq 200$ K: this trend is caused by the fact that the low energy excitations (below $\simeq$ 25 meV) increase on decreasing temperature although the high energy part does not change[32]. This yields a critical-like behavior which can be associated with the proximity of the AF quantum critical point. Furthermore, similar energy and temperature dependences are found for samples in the insulating phase nearby $x \simeq 0.4$[26, 27].

Quasi-dispersion

This normal contribution actually extends to higher energies and a significant spectral weight at energies comparable to J is observed[34, 75]. Furthermore, it has been recently reported in $YBCO_{6.5}$ that the high energy spin excitations exhibit a quasi-dispersion behavior. Above $\hbar\omega \sim 50$ meV, a double peak structure emerges from constant energy q-scans[34]. This evidences a noticeable inplane propagating character of the spin excitations as, at each energy, one can define a characteristic wave vector which varies and matches a dispersion curve reproduced in Fig. 14. Similarly to magnons in an ordered magnetic system, one then observes propagating excitations in the metallic phase of cuprates.

Using classical spin-wave formalism for an Heisenberg model (which in principle cannot apply to such non-magnetic ground-state), one can describe the observed dispersion as a softening of the magnon dispersion of the undoped materials (Fig. 14). From a simple parabolic fit, one deduces a spin velocity, c $\simeq$ 420 meV Å, 65% of the AF spin wave velocity of 650 meVÅ[37, 41]. This softening can be itself expressed in terms of an effective AF exchange as $J_{eff} \approx 0.65 J^{AF} \simeq 80$ meV at low temperature. A gap is found ~ 55 meV for the even excitations which slightly increases with temperature[34]. This even gap in the metallic state is found to be reduced from the magnon optical gap, $\omega_{opt}^{AF} = 67$ meV[40]. This effect can be readily accounted for by the same effective AF exchange using the classical spin-wave theory as, $\omega_{even} = 2\sqrt{J_{eff} J_{\perp}}$. However, as a limitation of this approach, counter-propagating excitations are not better resolved in the higher energy range[34]. Further, these observed peaks exhibit an intrinsic q-width which can be related to a real space correlation length of only about 9 Å. Therefore, instead of being well-defined propagating excitations, like magnons in the pure Néel state, one rather observes magnetic fluctuations which propagate only over small in-plane regions.

LSCO versus YBCO

Finally, it is instructive to compare the energy dependences of the spin response in LSCO near optimal doping (x ~ 0.15) and in weakly-doped underdoped $YBCO_{6.5}$. Above ~ 25 meV when the magnetic scattering becomes commensurate in LSCO[51], the neutron results show similar trends in the two systems. For instance, at about E ~ 50-60 meV, the magnetic spectrum is strongly reduced at (π, π)[5, 30, 32, 51]. This effect was previously attributed to an "high energy cut-off" but, more likely, this actually originates, at least in YBCO, due to the interplay of a few effects: first, above ~ 40 meV the spin susceptibility spectral weight at (π, π) effectively decreases with the energy. Moreover, $Im\chi$ displays a dip feature around 50 meV. Finally, the magnetic scattering strongly spreads out over the in-plane **q**-space for energies above 50 meV due to the quasi-dispersion behavior (Fig. 14). In LSCO, the quasi-dispersion has not been reported but, as a matter of fact, it can be inferred from high energy measurements for $x = 0.14$[75] as i) q-scan around E $\simeq$ 100 meV exbibits significant broadening compatible with propagating excitations ii) a zone boundary peak is found as one would expect from a dispersion-like behavior. In any case, one clearly observes in the two systems a similar momentum broadening at high energy.

Actually, to emphasize the comparison of the two systems, it is more convenient to perform the q-integration of the spin susceptibility over the 2D in-plane wave vector q_{2D}, as $Im\chi_{2D}(\omega) = \int d\mathbf{q}_{2D} Im\chi(\mathbf{q}_{2D}, \omega) / \int d\mathbf{q}_{2D}$. This also allows to overcome the difficulty that LSCO displays non overlapping incommensurate peaks below 25 meV. Further, the determination of $Im\chi$ in absolute units makes possible the direct comparison of LSCO ($x = 0.14$)[75] and $YBCO_{6.5}$[34]. The susceptibilities, calculated per single CuO_2-layer are reported in the same absolute units in Fig. 15. This q-integration has the effect to change the shape of the spin susceptibility as it enhances the high energy part due to the broadening in q-space of the AF fluctuations. For both systems, the spectral weight in the metallic state is very comparable to the spin wave spectral weight of the undoped materials (dashed lines in Fig. 15). The spin susceptibility exhibit a linear behavior at low energy, and then passes through a maximun around 25 meV, and extends to high energy. In YBCO, one finds in addition a dip feature around E$\simeq$ 50 meV[34] (whose origin is not clear at present) which actually might also exist in LSCO. Finally, apart from incommensurate peaks at low energy, both systems exhibit very

comparable momentum and energy dependences. As discussed above, modifications of $Im\chi$ in the SO state also show remarkable similarities. That strongly suggests that these two systems have same kind of hole doping per CuO_2 plane. In any case, this behavior is very different from the one observed in optimally doped YBCO. This is strongly suggesting that LSCO(x=0.15) does not correspond to an optimally doped cuprate in the generic phase diagram (Fig. 1).

Which models ?

What kind of models can explain these results in the normal state ? Some elements can be pointed out to describe at least part of the situation. First, these excitations can be associated with short range AF ordering of the localized copper spins. Indeed, the role played by localized copper spins in the metallic underdoped state is an important issue either for the nearly AF liquid model[7, 76] of in two dimensional quantum disordered approaches[68, 77, 78, 79]. Using RPA approximation, the magnetic exchange between copper spins $J(q)$ explains why the magnetic scattering is maximum at (π, π). Incidentally, the quasi-dispersion arises from $J(q)$ in this framework as heuristically discussed above. Further, an origin for the spin pseudogap is given in the t-J model[68, 78], which, similarly to what is found for the spin ladder compounds[79], occurs because of the formation of singlet RVB-states (spinon pairing). Second, these observations can also support itinerant magnetic models. As an example, it could remind the case of metallic Palladium where non-interacting electronic spin susceptibility is enhanced due to ferromagnetic interactions[80], leading to paramagnons behavior. In this approach, a dispersion-like behavior can simply occur due to the interplay of both band structure singularities and interaction renormalization. The observation of the even gap suggests the splitting of the Fermi surface caused by interlayer interaction. Interestingly, the even gap is shifted to low energies at higher doping[35]. Therefore, both dispersion curves in Fig. 14 tend to collapse at sufficiently high doping removing bands splitting. Such a doping dependence leads to an interesting issue regarding the photoemission experiments which have reported no "bilayer splitting" of the Fermi surface in $Bi_2Sr_2CaCu_2O_8$[13, 81]

10. CONCLUSION

The spin dynamics in metallic high-T_c cuprates as seen by Inelastic Neutron Scattering has been reviewed. Due the electronic interactions within a CuO_2-bilayer, one observes in the metallic state two different excitations: odd mode at lower energy (analogous of acoustic magnon) and even mode always weaker in amplitude (analogous of optical magnon). The odd susceptibility exhibits strong doping dependence which is characterized by two distinct contributions: a "magnetic resonance peak" which occurs only in the SC state, a normal contribution characterized by a spin pseudo-gap. Going into the overdoped regime in YBCO, the magnetic fluctuations in the normal state are strongly reduced[18]. Incidentally, it is very interesting to notice that the vanishing of magnetic correlations can be identified to the disappearance of the anomalous properties in overdoped cuprates (Fig. 1).

Using simple itinerant magnetism, it has been widely proposed that the resonance results from spin-flip charge carrier excitations across the SC energy gap. Such Fermi liquid approaches can also positively describe the normal state in the overdoped regime. It can even explain the occurence of incommensurate fluctuations in LSCO due to

nesting effect of the Fermi surface. However, other aspects of the spin dynamics in underdoped and optimally doped samples, and in particular, the existence of the spin pseudo-gap cannot be accounted for. More generally, the observation of peaks around (π, π) implies the existence of strong electronic correlations in the metallic regime.

Other interesting properties, which have not been addressed here, are the effect of impurities. Zinc substitution is known to strongly reduce the SC temperature without changing the hole amount in the CuO_2 planes. Interestingly, zinc also strongly modifies the spin excitation spectrum[26, 62, 82, 83]: with only 2 % of zinc, the resonance peak intensity is strongly reduced and low energy AF excitations appear where nothing was measurable in zinc-free samples[26, 62]. Most likely, these results suggest that zinc enhances the AF correlations and induces a localization of the charge carriers.

Finally, Inelastic Neutron Scattering experiments have evidenced unusual spin dynamics in metallic cuprates which shed new light on the strong electronic correlations in these materials. Nevertheless, the way the copper spins are intrinsically coupled to the holes remains a question under discussion and yields a very interesting problem of localized-itinerant duality magnetism. For sure, quantitative comparison of the spin susceptibility measured by NMR and INS is needed to understand that issue.

Acknowledgments

The work reviewed here is the fruit of the collaboration of many people whose names appear all along the references. Here, I want particularly to acknowledge my close collaborators: L.P. Regnault (CENG-Grenoble), Y. Sidis (LLB-Saclay), B. Hennion (LLB-Saclay), H.F. Fong (Princeton University), B. Keimer (Princeton University), H. Casalta (ILL-Grenoble) and A.S. Ivanov (ILL-Grenoble).

REFERENCES

1. J. Rossat-Mignot, L.P. Regnault, P. Bourges, P. Burlet, C. Vettier, and J.Y. Henry in *Selected Topics in Superconductivity*, Frontiers in Solid State Sciences Vol. 1., Edited by L.C. Gupta and M.S. Multani, (World Scientific, Singapore, 1993), p 265. Early "neutron" studies are referenced in [30].
2. For a recent Nuclear Magnetic Resonance review in cuprates, see C. Berthier, M.H. Julien, M. Horvatic, and Y. Berthier, Journal de Physique I (France), **6**, 2205 (1997).
3. A. Trokiner, this book; M. Mehring this book.
4. B. Batlogg, H.Y. Hwang, H. Takagi, R.J. Cava, H.L. Kao, and J. Kuo, Physica C, **235-240**, 130, (1994); B. Batlogg and V.J. Emery, Nature, **382**, 20. (1996). B. Batlogg, this book.
5. J. Rossat-Mignod, L.P. Regnault, C. Vettier, P. Bourges, P. Burlet, J. Bossy, J.Y. Henry, and G. Lapertot, Physica C**, 185-189,** 86 (1991).
6. N. Nagaosa, Science, **275**, 1078, (1997).
7. D. Pines, Z. Phys. B, **103**, 129 (1997); this book and references therein.
8. S.C. Zhang, Science, **275**, 1089, (1997).
9. F. Onufrieva, S. Petit, and Y. Sidis, Physica C, **266**, 101 (1996); Phys. Rev. B, 54, (1996); J. of Low Temp. Phys., **105**, 597 (1996).
10. J. Labbé, and J. Bok, Europhys. Lett, **3**, 1225 (1987); J. Bouvier, and J. Bok, Physica C, **249**, 117 (1995); this book.
11. C.M. Varma, Phys. Rev. B, **55**, 14554, (1997).
12. H. Ding, T. Yokoya, J.C. Campuzano, T. Takahashi, M. Randeria,, M.R. Norman, T. Mochiku, K. Kadowaki, and J. Giapintzakis, Nature, **382**, 51, (1996).
13. J.C. Campuzano, M. Randeria, M.R. Norman, and H. Ding, this book.

14. T. Ito, K. Takenaka, and S. Uchida. Phys. Rev. Lett. **70**, 3995, (1993).
15. R. Nemetschek, M. Opel, C. Hoffmann, P.F. Müller, R. Hackl, H. Berger, L. Forroó, A. Erb, and E. Walker, Phys. Rev. Lett. **78**, 4837, (1997); R. Hackl, this book.
16. F. Onufrieva, P. Pfeuty, and M. Kisselev, (SNS 97) to appear in J. Chem. Phys. Solids, (1998).
17. see e.g. G. Uimin, and J. Rossat-Mignot, Physica C, **199**, 251, (1992).
18. P. Bourges, L.P. Regnault, Y. Sidis, and C. Vettier, Phys. Rev. B, **53**, 876, (1996).
19. H. F. Fong, B. Keimer, P.W. Anderson, D. Reznik, F. Dogan, and LA. Aksay, Phys. Rev. Lett., **75**, 316 (1995).
20. Z.X. Shen, and J.R. Schrieffer, Phys. Rev. Lett. **78**, 1771, (1997).
21. M. Norman, H. Ding, J.C. Campuzanno, T. Takeuchi, M. Randeria, T. Yokoya, T. Takahashi, T. Mochiku, and K. Kadowaki, Phys. Rev. Lett. **79**, 3506, (1997) (cond-mat/9702144).
22. S.W. Lovesey, *Theory of Neutron Scattering from Condensed Matter*, Vol 1 & 2, (Clarendon, Oxford, 1984).
23. Neutron and Synchroton Radiation for Condensed Matter Studies, *Hercules, Ed. J. Baruchel, J.L. Hodeau, M.S. Lehmann, J.R. Regnard, and C. Schlenker*, (les Editions de Physique et Springer Verlag, 1993).
24. W. Reichardt, and L. Pintschovius, *Physical Properties of High Temperature Superconductors IV, ed by D.M. Ginsberg*, (World Scientific, 1993), p 295. W. Reichardt, J. of Low Temp. Phys., **105**, 807 (1996).
25. B. Keimer, N. Belk, R.J. Birgeneau, A. Cassanho, C.Y. Chen, M. Greven, M.A. Kastner, A. Aharony, Y. Endoh, R.W. Erwin, and G. Shirane, Phys. Rev. B, **46**, 14034 (1992).
26. Y. Sidis, thesis, University Paris-XI, Orsay (1995).
27. P. Bourges, Y. Sidis, B. Hennion, R. Villeneuve, G. Collin, and J. F. Marucco, Physica B, **213&214**, 54, (1995).
28. P. Dai, M. Yethiraj, H.A. Mook, T.B. Lindemer, and F. Dogan, Phys. Rev. Lett. **77**, 5425, (1996). P. Bourges, and L.P. Regnault, comment to Phys. Rev. Lett, to appear (1998).
29. H.A. Mook, M. Yehiraj, G. Aeppli, T.E. Mason, and T. Armstrong, Phys. Rev. Lett., **70**, 3490 (1993).
30. P. Bourges, L.P. Regnault, J.Y. Henry, C. Vettier, Y. Sidis, and P. Burlet, Physica B, **215**, 30, (1995).
31. P. Bourges, L.P. Regnault, Y. Sidis, J. Bossy, P. Burlet, C. Vettier, J.Y. Henry, and M. Couach, Europhysics Lett. **38**, 313 (1997).
32. L.P. Regnault, P. Bourges, P. Burlet, J.Y. Henry, J. Rossat-Mignod, Y. Sidis, and C. Vettier, Physica C, **235-240**, 59, (1994); Physica B, **213&214**, 48, (1995).
33. H.F. Fong, B. Keimer, D. Reznik, F. Dogan, and I. A. Aksay, Phys. Rev. B. **54**, 6708 (1996).
34. P. Bourges, H.F. Fong, L.P. Regnault, J. Bossy, C. Vettier, D.L. Milius, LA. Aksay, and B. Keimer, to appear in Phys. Rev. B, **56**, R11439, (1997) (cond-mat/9704073).
35. H.F. Fong, P. Bourges, *et al* to be published.
36. E. Manousakis, Rev. Mod. Phys. **63**, 1 (1991), and references therein.
37. S. Shamoto, M. Sato, J.M. Tranquada, B. Sternlieb, and G. Shirane, Phys. Rev. B, **48**, 13817(1993).
38. P. Bourges, H. Casalta, A.S. Ivanov, and D. Petitgrand, Phys. Rev. Lett. **79**, 4906, (1997) (cond-mat//9708060).
39. H. Eskes, and J.H. Jefferson, Phys. Rev. B, **48**, 9788 (1993).
40. D. Reznik, P. Bourges, H.F. Fong, L.P. Regnault, J. Bossy, C. Vettier, D.L. Milius, LA. Aksay, and B. Keimer, Phys. Rev. B **53**, R14741 (1996).
41. S.M. Hayden, G. Aeppli, T.G. Perring, H.A. Mook, and F. Dogan, Phys. Rev. B **54**, R6905 (1996).
42. A.J. Millis, and H. Monien, Phys. Rev. B, **54**, 16172, (1996).
43. O.K. Andersen, *et al*, J. Phys. Chem. Solids, **56**, 1579, (1995).

44. S. Chakravarty, A. Sudbo, P.W. Anderson, and S. Strong, Science, **261**, 337,(1993).
45. T.A. Kaplan, S.D. Mahanti, and Hyunju Chang, Phys. Rev. B **45**, 2565 (1992).
46. J.M. Tranquada, P.M. Gehring, G. Shirane, S. Shamoto, and M. Sato, Phys. Rev. B, **46**, 5561, (1992).
47. P. Bourges, L.P. Regnault, Y. Sidis, J. Bossy, P. Burlet, C. Vettier, J.Y. Henry and M. Couach, J. of Low Temp. Phys., **105**, 377 (1996).
48. P. Dai, H.A. Mook, and F. Dogan, preprint, (1997) (cond-mat/9707112).
49. B. J. Sternlieb, J.M. Tranquada, G. Shirane, S. Shamoto, and M. Sato, Phys. Rev. B, **50**, 12915 (1994).
50. T.E. Mason, G. Aeppli, and H.A. Mook, Phys. Rev. Lett., **68**, 1414 (1992); T.R. Thurston, P.M. Gehring, G. Shirane, R.J. Birgeneau, M.A. Kastner, Y. Endoh, M. Matsuda, K. Yamada, H. Kojima. and I. Tanaka, Phys. Rev. B, **46**, 9128 (1992).
51. S. Petit, A.H. Moudden, B. Hennion, A. Vietkin, A. Revcolevschi, Physica B, **234-236**, 800, (1997); Physica C, **282-287**, 1375, (1997).
52. Q. Si, Y. Zha, and K. Levin, Phys. Rev. B., **47**, 9055 (1993); Y. Zha, K. Levin, and Q. Si, *ibid*., **47**, 9124 (1993).
53. J.P. Lu et al Physica C, **179**, 191, (1991).
54. P.B. Littlewood *et al*, Phys. Rev. B., **48**, 487 (1993).
55. S.V. Maleyev, J. Phys. I. France, **2**, 181 (1992); S. Charfi-Kaddour, R-J. Tarento, and M. Héritier, J. Phys. I. France, **2**, 1853 (1992).
56. J.M. Tranquada, *et al*, Nature, **375**, 561, (1995).
57. V.J. Emery, and S.A. Kivelson, Physica C, **209**, 597, (1993).
58. J.R. Schrieffer, *Theory of Superconductivity*, (Frontiers in Physics (20), Addison Wesley), (1988).
59. H.F. Fong, B. Keimer, F. Dogan, and I.A. Aksay, Phys. Rev. Lett. **78**, 713 (1997).
60. J.M. Tranquada, W.J.L. Buyers, H. Chou, T.E. Mason, M. Sato, S. Shamoto, and G. Shirane, Phys. Rev. Lett. **64**, 800 (1990).
61. K. Yamada, *et al*, Phys. Rev. Lett. **75**, 1626, (1995).
62. Y. Sidis, P. Bourges, B. Hennion, L.P. Regnault, R. Villeneuve, G. Collin, and J.F. Marucco, Phys. Rev. B, **53**, 6811 (1996).
63. T.E. Mason, A. Schröder, G. Aeppli, H.A. Mook, and S.M. Hayden, Phys. Rev. Lett. **77**, 1604, (1996).
64. J. Rossat-Mignod, L.P. Regnault, P. Bourges, P. Burlet, C. Vettier, and J.Y. Henry, Physica B, **194&196**, 2131, (1994).
65. Y. Ohashi, and H. Shiba, J. Phys. Soc. Jpn., **62**, 2783 (1993); P. Monthoux, and D.J. Scalapino, Phys. Rev. Lett., **72**, 1874 (1994).
66. J. P. Lu, Phys. Rev. Lett., **68**, 125 (1992); N. Bulut, and D.J. Scalapino, Phys. Rev. B, **53**, 5149 (1996).
67. M. Lavagna, and G. Stemmann, Phys. Rev. B, **49**, 4235 (1994); G. Blumberg, B. P. Stojkovic, and M.V. Klein, Phys. Rev. B, **52**, R15741 (1995).
68. F. Onufrieva, and J. Rossat-Mignod, Phys. Rev. B, **52**, 7572 (1995). F. Onufrieva, Physica B, **215**, 41, (1995).
69. F. Onufrieva, Physica C, **251**, 348, (1995).
70. D.Z. Liu, Y. Zha, and K. Levin, Phys. Rev. Lett., **75**, 4130 (1995).
71. I.I. Mazin, and V. M. Yakovenko, Phys. Rev. Lett., **75**, 4134 (1995).
72. L. Yin, S. Chakravarty and P.W. Anderson, Phys. Rev. Lett., **78**, 3559 (1997).
73. E. Demler, and S.C. Zhang, Phys. Rev. Lett., **75**, 4126 (1995).
74. L.P. Regnault, I. Zaliznyak, J.P. Renard, and C. Vettier, Phys. Rev. B **50**, 9174 (1994).
75. S.M. Hayden, G. Aeppli, H.A. Mook, T.G. Perring, T.E. Mason, S-W. Cheong and Z. Fisk, Phys. Rev. Lett. **76**, 1344 (1996).
76. V. Barzykin, D. Pines, A. Sokol, and D. Thelen, Phys. Rev. B, **49**, 1544 (1994).
77. A.J. Millis and H. Monien, Phys. Rev. B **50**, 16606 (1994).
78. T. Tanamoto, H. Kohno, and H. Fukuyama, J. Phys. Soc. Jpn., **61**, 1886 (1992); G.

Steinmann, C. Pepin, and M. Lavagna, Phys. Rev. B, **50**, 4075. (1994).
79. T.M. Rice, S. Gopalan, and M. Sigrist, Europhys. Lett., **23**, 445. (1993).
80. R.M. White, Quantum Theory of Magnetism, *in* springer series to Solid-state Science, **32**, Springer Verlag Berlin (1983).
81. H. Ding, *el al*, Phys. Rev. Lett., **76**, 1533, (1996).
82. K. Kakurai, S. Shamoto, T. Kiyokura, M. Sato, J. M. Tranquada, and G. Shirane, Phys. Rev. B. **48**, 3485 (1993). H. Harashina, S. Shamoto, T. Kiyokura, M. Sato, K. Kakurai, and G. Shirane, J. Phys. Soc. Jpn **62**, 4009 (1993).
83. P. Bourges, Y. Sidis, B. Hennion, R. Villeneuve, G. Collin and J.F. Marucco, Czechoslovak Journal of Physics, **46**, 1155 (1996). P. Bourges, Y. Sidis, L.P. Regnault, B. Hennion, R. Villeneuve, G. Collin, C. Vettier, J.Y. Henry, and J.F. Marucco, J. Phys. Chem. Solids, **56**, 1937, (1995).